Proceedings World Geothermal Congress 2026
Calgary, Canada, June 8 – 11, 2026

Evolution of slip behaviors and hydraulic properties during hydraulic and mechanical shearing

Xiang-Zhao Kong[1]*, Nikita Bondarenko[1], Alexandra Aregger[1], and Paul Selvadurai[2]
[1]Geothermal Energy and Geofluids (GEG), Department of Earth and Planetary Sciences, ETH Zürich [2]Swiss Seismological Service, ETH Zürich, Zürich, Switzerland
*xkong@ethz.ch

Keywords: Slip, permeability, rupture energy, energy partition, acoustic emission

ABSTRACT

Fracture reactivation has become a key technique for enhancing the transmissivity of low-permeability rock formations. Numerous studies have endeavored to elucidate the key parameters influencing fracture reactivation, encompassing fault roughness, fault mineralogy, stress state, injection rate, injection volume, fluid properties, and fluid-rock interactions. Nonetheless, substantial gaps persist in comprehending the interrelationships among rupture energy, injection schemes, slip behavior, and resultant permeability. This study investigates reactivation and rupture processes in pre-fractured Westerly granite using a triaxial flow-through system, focusing on partitioning of energy between frictional sliding, creation of new fractures, and how it affects evolution of permeability and acoustic emission (AE) activity. Two samples, one with a rough natural fracture and one with a smooth saw-cut surface, were subjected to mechanical loading and controlled fluid injection in order to trigger slip on the pre-existing fracture. Multiple stick-slip and dynamic rupture events were produced, including the formation of secondary fractures.

The results show that AE energy correlates with rupture energy during slow slip events, whereas no systematic variation in rupture energy is observed between mechanically and fluid-induced dynamic events. Mechanically induced stick-slip events tend to display increasing rupture energies with accumulated slip distance, while permeability evolution shows no consistent trend because of the competing effects of fracture dilation and compaction, gouge formation, and secondary fracturing. Together, these observations highlight the complex interplay between rupture energy, permeability changes, and AE release, providing insight into fault reactivation processes and their implications for subsurface fluid flow and the mitigation of injection-induced seismicity.

1. INTRODUCTION

Fracture reactivation has been reported in a wide range of subsurface applications, including enhanced geothermal systems (EGS) (Evans et al., 2005; Evans, 2005; Häring et al., 2008; Hofmann et al., 2019), geological carbon sequestration (Hajiabadi et al., 2021), wastewater disposal (Kolawole et al., 2019; Mei et al., 2021), and hydrocarbon production in tight reservoirs (Lei et al., 2017). Through controlled mechanical or hydraulic stimulation, fracture reactivation has become a key technique for enhancing the transmissivity of low-permeability rock formations (Jones et al., 2024; Meier & Zingg, 2025; Ricks et al., 2025). By increasing pore pressure or applying external stress, pre-existing fractures can be reactivated, thereby improving fluid connectivity within the reservoir. Reactivation may occur as tensile opening, as shear slip—representing relative sliding along the fracture plane (Stober, 2021)—or as a combination of both. Optimizing this process requires a comprehensive understanding of how fractures deform, transmit fluids, and release stored energy under controlled stimulation conditions.

Despite decades of laboratory and field research, the coupled mechanisms governing fracture reactivation remain incompletely understood. Numerous studies have examined how parameters such as fracture roughness, mineralogy, stress state, injection rate, and fluid–rock interactions influence permeability evolution (Ye and Ghassemi, 2018; Ishibashi et al., 2023; Ji et al., 2023). However, the underlying processes that control how stored elastic energy is released and partitioned among frictional slip, microfracturing, and seismic radiation remain elusive. Because energy partitioning determines both the mechanical stability of fractures and their capacity to transmit fluids, resolving this gap is crucial for predicting the hydromechanical and seismic outcomes of stimulation.

This study experimentally investigates shear slip on pre-existing fractures triggered by either fluid injection or mechanical loading, with a focus on the partitioning of energy during stress accumulation and release. Special

emphasis is placed on identifying the mechanisms through which stored elastic energy is redistributed among frictional sliding, fracture propagation, and radiated seismic energy. We additionally examine the concurrent evolution of fracture permeability and acoustic emission (AE) activity to link these observations to the underlying energy dissipation processes.

2. METHODOLOGY

Two samples of pre-fractured Westerly granite (WG1 and WG2) were investigated using triaxial flow-through experiments (Figure 1). Sample WG1 was prepared (saw-cut) with two opposing notches oriented at an angle of α = ~40° to the principal loading axis (σ_1), each about 10-15 mm in length, to promote controlled tensile fracture development using a radial point load. Sample WG2 was saw-cut completely at an angle of α = ~55° to the principal loading axis (σ_1). The fracture surfaces were subsequently abraded using a #80 sandpaper to introduce a controlled and homogeneous roughness.

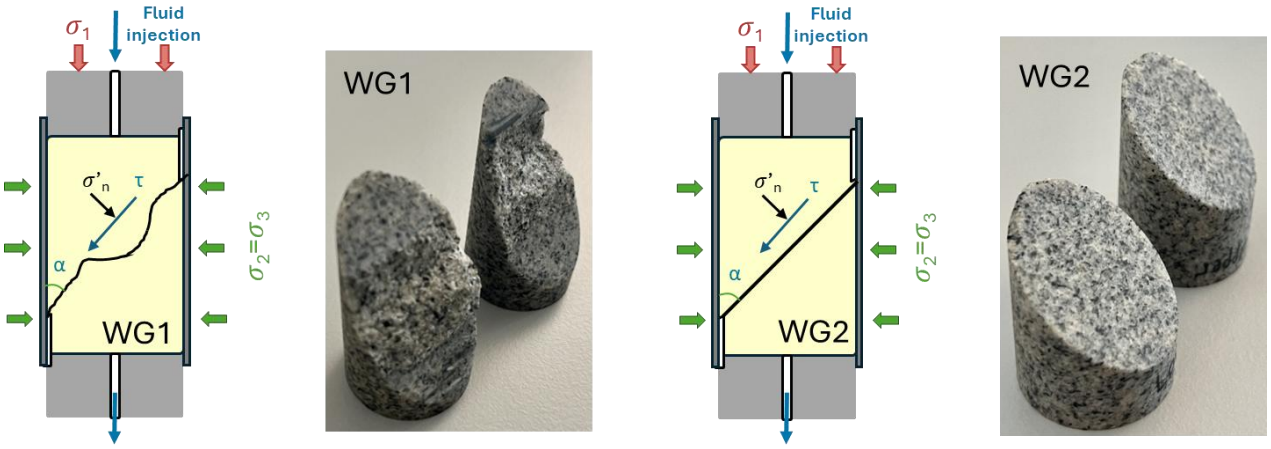


Figure 1. Schematic experimental setup and the two pre-fractured granite samples.

When samples were hosted in the triaxial cell, WG1 has a length of 50.8 mm and a diameter of 25.4 mm, while WG2 has the same diameter but is shorter (45.9 mm). To ensure that the injected fluid is directed into the pre-existing fracture, two small rectangular (~4 x 15 mm^2) pieces of metal mesh were attached to the sample walls at both ends, bridging the gap between the fracture inlet/outlet and the sample end faces (Figure 1). During the experiments, samples were enclosed in a Viton rubber jacket to isolate them from the confining fluid and to enable the application of lateral stress (σ_2= σ_3).

Throughout the tests, multiple physical parameters were continuously acquired, including axial and radial stress, pore fluid pressure, axial displacement, acoustic emission (AE) signals, flow rate, and injected volume. During the WG1 experiment, four slip events were observed: the first two were mechanically-induced under drained conditions by applying axial load, and the latter two were fluid-injection reactivated through stepwise increase in pore fluid pressure. The WG2 experiment comprised a sequence of mechanically induced stick-slip events, followed by four fluid-injection reactivated slips.

3. RESULTS

At the start of the experiment, WG1 was confined to σ_2= σ_3= 3 MPa radial and σ_1 = 5 MPa axial pressure (Figure 2). A constant fluid injection rate of 7 ml/min was maintained. The sample was loaded axially in displacement-control mode until the first dynamic slip occurred. During the subsequent relaxation phase, a pronounced increase in pore pressure was observed. The second event was triggered by repeating axial loading and occurred in a quasi-static manner. After axial unloading and permeability measurement, the sample was again axially loaded close to failure, after which pore pressure was increased stepwise via downstream pressure control to induce the third slip. The same procedure was repeated for the fourth event. After each slip event, WG1 was unloaded to the same state of stress (σ_1 = 4.2 MPa and σ_2= σ_3 = 3 MPa) for permeability measurement under identical environmental conditions (i.e., the same shear and effective normal stress acting on the pre-existing fracture). Post-experimental examination with X-ray CT scans revealed that deformation in WG1 was not restricted to a single fracture surface but produced a complex damage zone. A dominant oblique fracture, corresponding to the reactivation plane, cuts across the sample and is accompanied by extensive branching cracks, particularly visible in slices a and b in Figure 2.

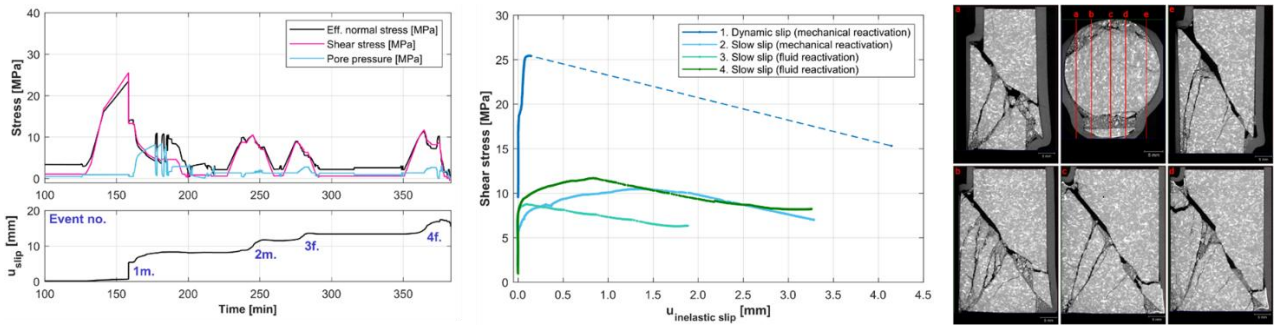


Figure 2. The WG1 experiment. Left: Evolution of shear stress (τ), effective normal stress (σ_n'), pore fluid pressure, and slip displacement (u_{slip}) along the fracture plane, marked with the four slip events (m and f denotes mechanical and fluid reactivation, respectively). Middle: Shear stress-inelastic slip displacement of individual slip events. Right: CT scan images of WG1 after the experiment. The central image shows a horizontal cross-section through the cylinder with red lines marking the locations of five vertical slices (a–e) parallel to the loading axis.

Sample WG2 was first subjected to a confining pressure of $\sigma_2 = \sigma_3 = 3$ MPa radial, maintained constant throughout the test, and to an axial stress of $\sigma_1 = 3.2$ MPa. Steady-state fluid flow was then maintained by running the upstream pump at constant flow rate of 5 ml/min, while the downstream pump was operated in pressure-control mode to hold the prescribed back pressure (Figure 3). Events #1-#8 and #10-#11 are stick-slip events, triggered by mechanical loading via a constant displacement rate of the pump piston of 0.01 MPa/s. Events #9, #13, and #14 are triggered by increasing the back pressure in a stepwise manner, while the flow-through injection rate was kept constant, presenting as "drained injection"-induced events. Event #12 is triggered at the same inflow rate while the downstream is closed, presenting as "undrained injection"-induced event. X-ray CT scans of sample WG2 show that deformation was not confined to the original saw-cut fracture but produced a complex fracture network (Figure 3). In addition to the smooth saw-cut surface, a major conjugated fracture developed at an angle of ~27° to the principal axis, most likely associated with the large dynamic slip event #14.

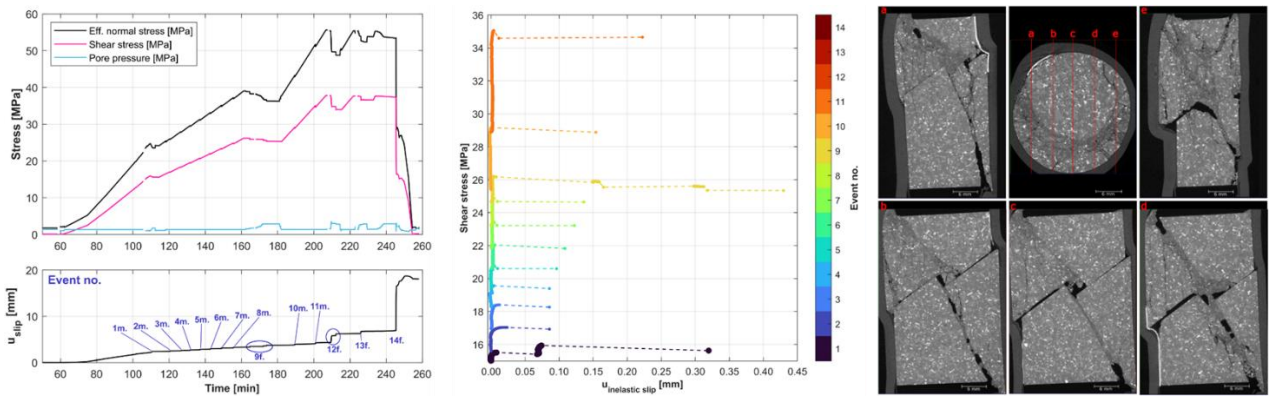


Figure 3. The WG2 experiment. Left: Evolution of shear stress (τ), effective normal stress (σ_n'), pore fluid pressure, and slip displacement (u_{slip}) along the fracture plane, marked with the fourteen slip events (m and f denotes mechanical and fluid reactivation, respectively). Middle: Shear stress-inelastic slip displacement of individual slip events. Right: CT scan images of WG1 after the experiment. The central image shows a horizontal cross-section through the cylinder with red lines marking the locations of five vertical slices (a–e) parallel to the loading axis.

The WG1 experiment (rough fracture) produced four slip events (Figure 2 and Figure 4). In all cases, post-peak rupture energy exceeded pre-peak values. The first and third events were strongly post-peak dominated (96% and 90%), while the second and fourth showed more balanced partitioning (≈45–60%) (Figure 4).

The WG2 experiment (smooth, saw-cut fracture) produced fourteen slip events. Rupture energy partitioning (Figure 4) is shown for events] #1–#13; event #14 was excluded due to its large slip (≈13.8 mm) and entirely post-peak energy release (Figure 3). In the first three events, pre-peak rupture energy contributed 11–23% of the total, while in later events it dropped below 10%, indicating predominantly post-peak dissipation. $G_{c,pre}$ decreased up

to event #5, whereas $G_{c,post}$ declined only until event #2 before rising again. Event #12 stands out, showing an unusually high $G_{c,pre}$ exceeding that of all mechanically reactivated slips (Figure 4).

In the rough fracture experiment (WG1), AE energy exhibits a clear positive correlation with rupture energy: events associated with higher rupture energy also dissipated more energy as acoustic emission. This relationship is evident in both pre-peak and post-peak stress stages, though the majority of AE energy was recorded in post-peak stage (Figure 4). For the smooth saw-cut fracture (WG2), no systematic relationship between AE activity and rupture energy could be established. Most stick-slip events produced only a single AE signal, often clipped above the sensor threshold, making quantitative energy estimates unreliable. The scarcity of detectable AE activity suggests that smooth fractures experience less asperity breakdown and grain crushing, and therefore generate fewer seismic emission during slip.

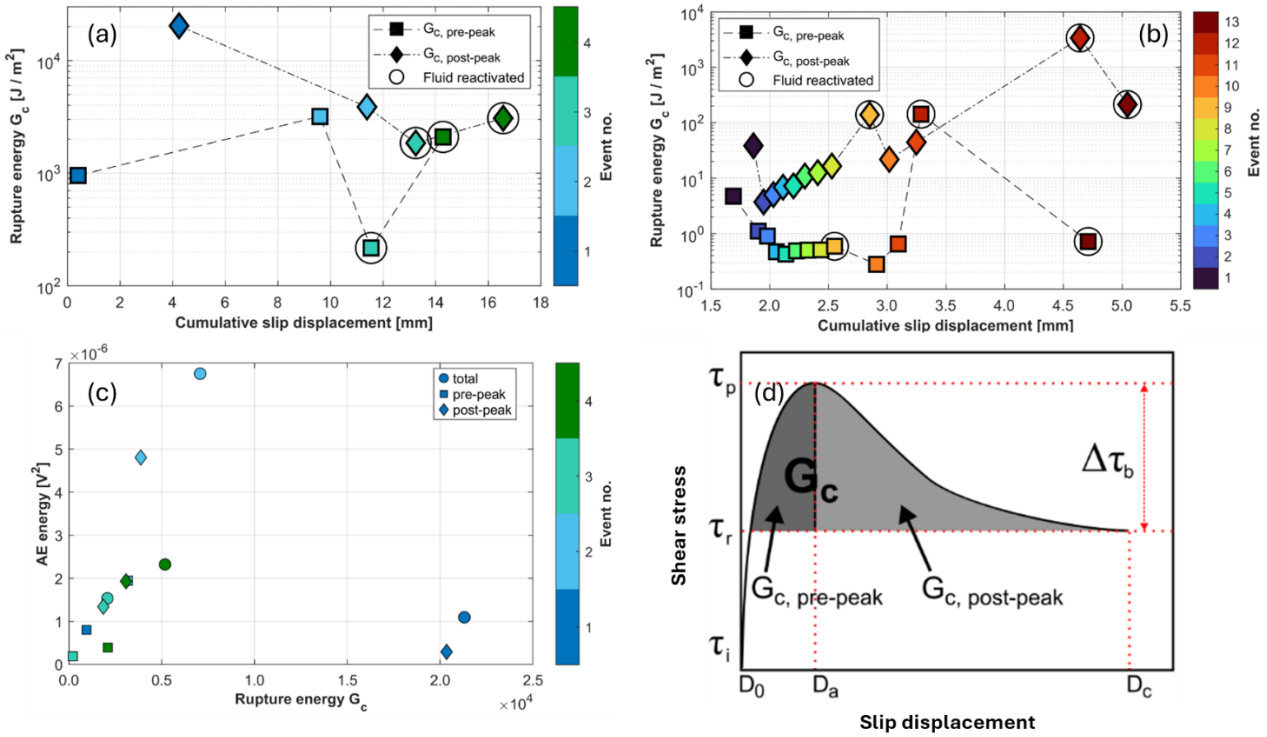


Figure 4. Rupture energy and its partitioning. (a) Partitioning of rupture energy G_c versus cumulative slip displacement for individual events in WG1. (b) Partitioning of rupture energy G_c versus cumulative slip displacement for individual events in WG2. (c) AE energy versus rupture energy in experiment WG1. (d) Following Ohnaka et al. (1997), rupture energy, $G_c = G_{c,pre} + G_{c,post}$, defined as the area beneath the shear stress-slip displacement curves, where the inelastic displacement is defined as the difference between the breakdown slip displacement, D_c, and the initial slip displacement, D_0.

4. DISCUSSION

Our experiments on rough and smooth fractures revealed that rupture energy partitioning depends strongly on fracture morphology, loading mode, and pore-pressure evolution.

In mechanically induced slips, rough fractures showed an initial decrease in rupture energy, consistent with asperity degradation and surface smoothing, followed by an increase during the final fluid-induced event, indicating renewed microfracturing and dilation. Smooth saw-cut fractures, by contrast, did not exhibit a monotonic trend—after an initial drop, rupture energy gradually increased with repeated slip. Fluid-induced reactivations introduced further variability, highlighting the influence of injection strategy and transient pore-pressure redistribution on fault stability and energy release.

Comparing loading modes shows that mechanical reactivation leads to systematic, friction-dominated behavior, whereas fluid reactivation promotes heterogeneous rupture by locally reducing effective normal stress and triggering microfracturing or tensile opening. Consequently, fluid-driven slips display a broader range of rupture energies and more complex energy partitioning.

Acoustic emission analysis supports this interpretation: AE activity in rough fractures correlated well with rupture energy, particularly during post-peak stages where asperity breakdown dominated. In smooth fractures, however, AE signals were sparse and clipped, indicating limited asperity interaction and less high-frequency radiation.

Hydraulic resistance exhibited no clear relation to rupture energy, instead reflecting transient local processes such as dilation, compaction, and gouge redistribution. We thus don't produce an associated figure in this paper. These findings emphasize that fracture transmissivity evolves through coupled mechanical and hydraulic effects that cannot be captured by energy release alone.

Overall, the results demonstrate that frictional sliding and new fracturing are not distinct processes but concurrent and interdependent. Their relative contributions shift dynamically as slip progresses, influenced by roughness, loading conditions, and fluid pressurization. Understanding this evolving energy partitioning is essential for predicting fracture stability, permeability evolution, and induced seismicity in subsurface systems.

Acknowledgements

The Werner Siemens Foundation (Werner Siemens-Stiftung) is thanked for its support of the Geothermal Energy and Geofluids (GEG.ethz.ch) Group at ETH Zurich.

REFERENCES

Evans, Keith F.: Permeability creation and damage due to massive fluid injections into granite at 3.5 km at Soultz: 2. Critical stress and fracture strength, Journal of Geophysical Research: Solid Earth 110, no. B4 (2005).

Evans, Keith F., Albert Genter, and Judith Sausse.: Permeability creation and damage due to massive fluid injections into granite at 3.5 km at Soultz: 1. Borehole observations, Journal of Geophysical Research: Solid Earth 110, no. B4 (2005).

Hajiabadi, Seyed Hasan, Pavel Bedrikovetsky, Sara Borazjani, and Hassan Mahani.: Well Injectivity during CO_2 geosequestration: a review of hydro-physical, chemical, and geomechanical effects, Energy & Fuels 35, no. 11 (2021): 9240-9267.

Hofmann, Hannes, Günter Zimmermann, Marton Farkas, Ernst Huenges, Arno Zang, Maria Leonhardt, Grzegorz Kwiatek et al.: First field application of cyclic soft stimulation at the Pohang Enhanced Geothermal System site in Korea, Geophysical Journal International, 217, no. 2 (2019): 926-949.

Häring, Markus O., Ulrich Schanz, Florentin Ladner, and Ben C. Dyer.: Characterisation of the Basel 1 enhanced geothermal system, Geothermics, 37, no. 5 (2008): 469-495.

Ishibashi, Takuya, Hiroshi Asanuma, Yusuke Mukuhira, and Noriaki Watanabe.: Laboratory hydraulic shearing of granitic fractures with surface roughness under stress states of EGS: Permeability changes and energy balance, International Journal of Rock Mechanics and Mining Sciences 170 (2023): 105512.

Ji, Yinlin, Wei Zhang, Hannes Hofmann, Frédéric Cappa, and Supeng Zhang.: Fracture permeability enhancement during fluid injection modulated by pressurization rate and surface asperities, Geophysical Research Letters 50, no. 18 (2023): e2023GL104662.

Jones, Clay, Stuart Simmons, and Joseph Moore.: Geology of the Utah frontier observatory for research in geothermal energy (forge) enhanced geothermal system (egs) site, Geothermics, 122 (2024): 103054.

Kolawole, Folarin, C. S. Johnston, C. B. Morgan, J. C. Chang, K. J. Marfurt, David A. Lockner, Ze'ev Reches, and B. M. Carpenter.: The susceptibility of Oklahoma's basement to seismic reactivation, Nature Geoscience 12, no. 10 (2019): 839-844.

Lei, Xinglin, Dongjian Huang, Jinrong Su, Guomao Jiang, Xiaolong Wang, Hui Wang, Xin Guo, and Hong Fu.: Fault reactivation and earthquakes with magnitudes of up to Mw4. 7 induced by shale-gas hydraulic fracturing in Sichuan Basin, China, Scientific reports 7, no. 1 (2017): 7971.

Mei, Wenrong, Ammal F. Al-Anazi, and Karam S. Yateem.: Water Disposal Wells Injectivity Enhanced by Well Treatment Optimization, In Offshore Technology Conference, p. D041S054R003. OTC, 2021.

Meier, P., and O. Zingg: Status of Multi-Stage EGS and the Haute-Some Project in Canton Jura, Switzerland, In 86th EAGE Annual Conference & Exhibition, vol. 2025, no. 1, pp. 1-5. European Association of Geoscientists & Engineers, 2025.

Ohnaka, M., M. Akatsu, H. Mochizuki, A. Odedra, F. Tagashira, and Y. Yamamoto.: A constitutive law for the shear failure of rock under lithospheric conditions, Tectonophysics 277, no. 1-3 (1997): 1-27.

Ricks, Wilson, Katharine Voller, Gerame Galban, Jack H. Norbeck, and Jesse D. Jenkins: The role of flexible geothermal power in decarbonized electricity systems, Nature Energy, 10, no. 1 (2025): 28-40.

Stober, K. B.: Geothermal Energy-From Theoretical Models to Exploration and Development. 2021. Switzerland: Springer Cham.

Ye, Zhi and Ahmad Ghassemi.: Injection-induced shear slip and permeability enhancement in granite fractures, Journal of Geophysical Research: Solid Earth 123, no. 10 (2018): 9009-9032.